

Characterisation of a ΔE – E particle telescope using the ANSTO heavy ion microprobe

Rainer Siegele^{a,*}, Mark Reinhard^a, Dale Prokopovich^a, Mihail Ionescu^a,
David D. Cohen^a, Anatoly B. Rosenfeld^b, Iwan M. Cornelius^b, Andrew Wroe^b,
Michael L.F. Lerch^b, A. Fazzi^c, A. Pola^c, S. Agosteo^c

^a Environment Division, Australian Nuclear Science and Technology Organisation, New Illawarra Road, PMB 1, Menai 2234, NSW, Australia

^b Centre for Medical Radiation Physics, University of Wollongong, Northfields Avenue, NSW 2522, Australia

^c Dipartimento di Ingegneria Nucleare, Politecnico di Milano, via Ponzio 34/3, I-20133, Milano, Italy

Available online 14 February 2007

Abstract

Semiconductor planar processing technology has spurred the development of novel radiation detectors with applications in space, high energy physics, medical diagnostics, radiation protection and cancer therapy. The ANSTO heavy ion microprobe, which allows a wide range of ions to be focused into spot sizes of a few micrometers in diameter, has proven to be an essential tool for characterising these detectors using the Ion Beam Induced Charge (IBIC) imaging technique. The use of different ions and the wide range of available energies on the heavy ion microprobe, allows the testing of these devices with ionising particles associated with different values of linear energy transfer (LET).

Quadruple coincidence measurements have been used to map the charge collection characteristics of a monolithic ΔE – E telescope. This was done through simultaneous measurement of the spatial coordinates of the microbeam relative to the sample and the response of both detector elements. The resulting charge collection maps were used to better understand the functionality of the device as well as to ascertain ways in which future device designs could be modified to improve performance.

© 2007 Elsevier B.V. All rights reserved.

PACS: 07.77.–n; 87.53.Rd; 29.40.Wk

Keywords: Microprobe; Microdosimetry; Particle telescope

1. Introduction

Solid state detectors have found a wide range of applications in radiation dosimetry over the past decade. Silicon based detectors offer a significant advantage over conventional ionisation chambers, because they can be manufactured with much smaller dimensions and a number of these devices can easily be arranged in arrays. This offers the opportunity to measure variations in the energy deposition of the radiation on millimetre or sub-millimetre scale.

Most effects of radiation, especially biological effects, depend on the microscopic distribution of the energy deposition. This can be seen by that fact, that the biological effectiveness of otherwise equal doses of different types of radiation are quite dissimilar. Microdosimetry, the study of microscopic fluctuations in energy deposition, tries to provide a description of the spatial distribution of absorbed energy in irradiated matter.

Research into microdosimetry using silicon devices has been pioneered by Dicello et al. [1] and Rosenfeld et al. [2]. More recently Agosteo et al. [3] suggested the use of a ΔE – E telescope coupled with a converter as a microdosimeter in neutron fields. This study investigates the charge collection properties of the ΔE – E telescope, in particular

* Corresponding author. Tel.: +61 2 9717 3967; fax: +61 2 9717 3257.
E-mail address: rns@ansto.gov.au (R. Siegele).

the boundaries of the ΔE region and the influence of radiation damage.

Ion microprobes have proven useful for investigating the charge collection properties of semiconductor radiation detectors [4,5]. In microdosimeters edge effects become important, because the size of the active volume is small compared to the edge area of the device. This makes it necessary to test the detector response to radiation on a microscopic scale, which can be done using a focussed ion beam, with a size comparable to the feature size of the device. To use a microdosimeter in clinical applications, it is necessary to measure the detector response to a range of ions, which requires an ion microprobe capable of focusing a wide range of elements, such as ANSTO's heavy ion microprobe [6].

At ANSTO various studies have already been undertaken investigating the response of various types of detectors and dosimeters to ion irradiation using Ion Beam Induced Current (IBIC) measurements [7–9]. However, in order to investigate the correlation between the E and ΔE signals of ΔE – E telescope, this study requires coincidence data acquisition of the two signals, together with the beam position information from the microprobe.

2. Experimental

The device studied in this investigation is a monolithic ΔE – E detector, which was developed as a particle telescope for intermediate nuclear physics experiments. It consists of a ΔE and an E stage with a thickness of approximately 1 μm and 500 μm , respectively. An electron micrograph of the ΔE – E telescope is shown in Fig. 1. The figure clearly shows the contact pads in the four corners of the device. The bottom two are for the common p+ cathode as well as the ΔE -detector n+ anode. The top contacts are for an additional guard rings surrounding the device. A cross section of the device is shown as an insert.

The sensitive area of the device is about 1 mm². The device is made on a high resistivity n-type silicon wafer with a buried p+ type implantation (common cathode). The ΔE and E anodes were made by As and P implantation from the front and back surfaces, respectively. On top of the ΔE stage of the detector is a ~ 0.2 μm thick metal dead layer [3].

In order to investigate the response for a range of ion beams and different linear energy transfer (LET) values, the device was tested at the ANSTO high energy heavy ion microprobe using 2 and 3 MeV H, 3 MeV He as well as 12 and 20 MeV C beams. The LET values for these beams vary from 0.09 MeV/(mg/cm²) to 4.4 MeV/(mg/cm²) for 3 MeV H and 12 MeV C, respectively, while the projected range varies from 100 to 11 μm . This range is well within the thickness of the E stage of the detector and thus ensures the complete energy deposition in the active volume.

The ion beam was focused to spot sizes between $1 \times 1 \mu\text{m}^2$ and $2 \times 2 \mu\text{m}^2$, using the Oxford triplet

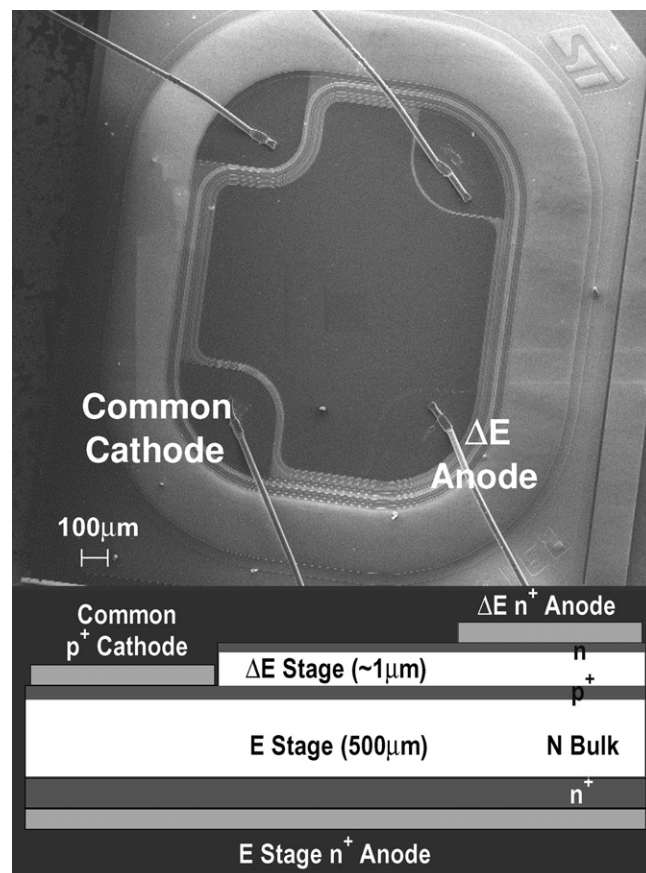


Fig. 1. Micrograph of the ΔE – E telescope. The micrograph clearly shows the 4 contact pads in the corners of the device. The insert shows a cross section of the device across the common cathode and the ΔE anode in the lower section of the device.

(OM155), varying slightly for different ions. This spot size resulted in 500–1000 ions hitting the sample per second. For each ion penetrating the detector, the amount of charge created in the ΔE and E stage of the detector is measured separately using two charge sensitive preamplifiers (AMPTEK A250). To minimise the noise both pre-amplifiers are mounted close to the device in the vacuum chamber. Coincidence ΔE and E signals were recorded together with the x and y position information of the beam. This quadruple coincidence enables us to later analyse the data offline by various criteria.

3. Results and discussion

Fig. 2 shows the ΔE – E coincidence spectrum for different beam energies and ions. Fig. 2(a) shows spectra for 2 MeV H and 3 MeV He, while Fig. 2(b) shows spectra for carbon beams at 12 and 20 MeV. The measurements were taken in the centre of the device to avoid edge effects and give the true performance of the device. The ion beam was scanned over an area between 70 and 100 μm , depending on the magnetic rigidity of the ions.

The two figures have different energy scales, because of the vast differences in the energies deposited in both the

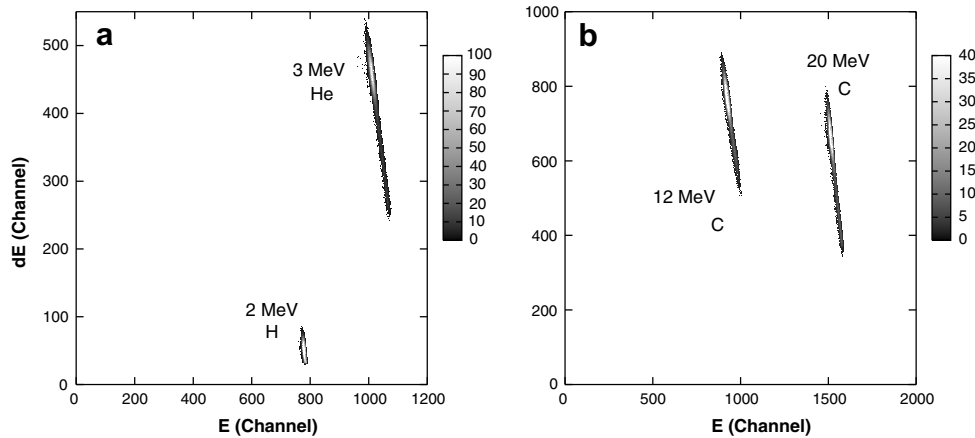


Fig. 2. ΔE - E coincidence maps taken at the centre of the ΔE - E telescope for different ions and energies (2 MeV H, 3 MeV He, 12 MeV and 20 MeV C).

dE and E part of the detector for the different ions. In fact for 2 MeV H the energy deposited in the ΔE part of the detector is close to the noise limit of the system, which is the reason why a spectrum for 3 MeV H, which was another beam used in this study, is not shown here. The figures demonstrate how different ions can be separated, by these ΔE - E coincidence measurements in the detector.

With the exception of hydrogen all coincidence spectra show a tail both in the E and ΔE detector signal. While this tail is on the low energy side for the ΔE spectrum it is as the high energy side of the peak for the E spectrum. This suggests that both tails are correlated, that is, events in the two tails originate from the same particles. The ΔE - E coincidence spectra clearly demonstrate that this is the case. The low energy part of the ΔE spectrum comes in deed from the same ions that form the high energy part of the E spectrum. Hence these tails can only be attributed to processes that result in energy deposition shifted from the ΔE detector to the E detector.

This can either be channelling of ions in the silicon crystal of the ΔE detector, thickness variations in the ΔE part of the detector, or charge funneling into the E stage. Large

scale thickness variations can be tested by plotting the distribution of events, which are in the tail of the ΔE - E coincidence spectrum as a function of the beam position. These maps show a random distribution across the analysis area for both peak and the tail of the coincidence spectrum. However, thickness variations, caused by any roughness of the top and bottom interface of the ΔE detector can not be seen in the maps if they are short range. Nevertheless, this is expected to lead to a broadening of the peak and not just a tail on the low energy end of the ΔE signal. Hence thickness variations in the ΔE part of the detector can be ruled out as a cause of the tail. The random distribution of events from different parts of the energy spectrum across the scan area, demonstrates the uniformity of the thickness of the ΔE detector.

Analysis of the spectra shows, that between 15% and 20% of events are in the tail of the spectrum, regardless of the ion used. Hydrogen is an exception, because the energy loss in the ΔE detector is too small for any energy variations to be resolved. If channelling is causing the tails then 15–20% of ions are in the channeled fraction of the beam. Lugujo and Mayer [10] have shown that even after

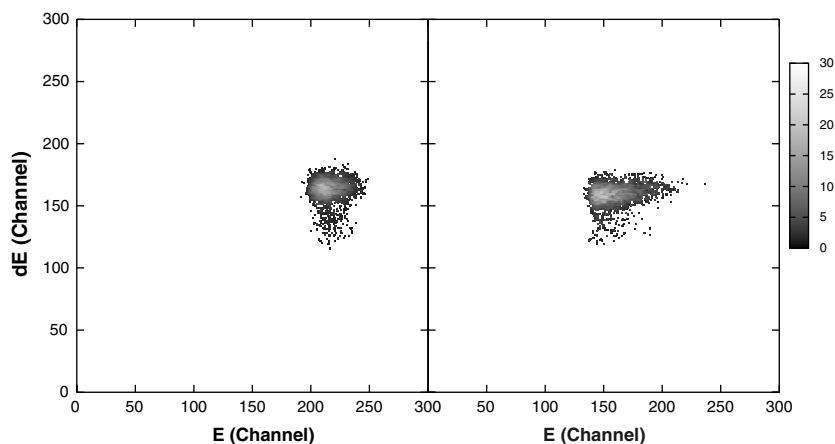


Fig. 3. ΔE - E coincidence spectra of 12 MeV C take on the same spot for 10^4 particles. The second spectrum was taken after 10^5 events, in a beam spot size of $2 \times 2 \mu\text{m}^2$. The spectrum shows a clear shift in the signal of the E part of the detector.

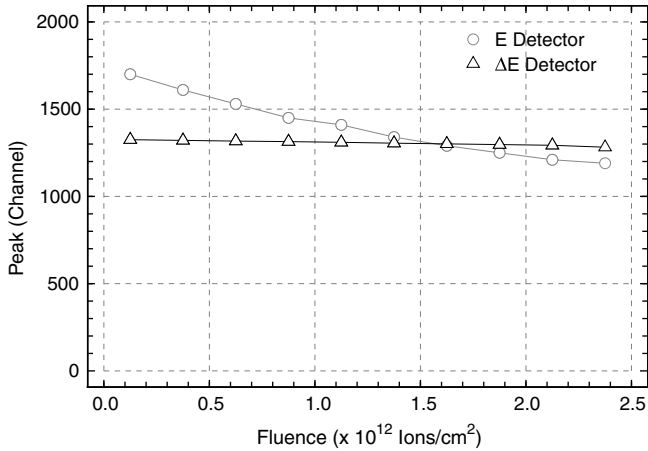


Fig. 4. Energy shift of E and ΔE peaks as a function of ion fluence for 12 MeV C.

traversing through a $0.2 \mu\text{m}$ thick Al layer a large fraction of the beam can still be channeled.

Only limited work was undertaken with heavy ions, because of the damage introduced by heavy ions. Fig. 3 demonstrates the damage introduced by the focused ion beam. In this case the beam was not scanned, but was kept stationary in one spot. Fig. 3 shows ΔE – E coincidence spectra taken at an undamaged spot (left) and after 10^5 ions (right). In each spectrum the signal for 10^4 particles was collected.

The right figure shows the damage introduced in a $2 \times 2 \mu\text{m}^2$ area by 10^5 ions of 12 MeV carbon, which is equivalent to 2.5×10^{12} particles/ cm^2 . 12 MeV is the ion beam with the highest LET of all the ion beams tested, with an energy loss of $4.4 \text{ MeV}/(\text{mg}/\text{cm}^2)$. Fig. 4 shows the peak position for the E and ΔE signal as a function of the fluence. The figure shows an almost 30% decrease in the energy signal, which is due to the damage introduced by the ions. This damage leads to trapping of the charge and thus a reduced signal size. However, the spectrum of

the ΔE detector shows only a very small change in the peak position. This can be explained by the fact that the ΔE stage is only about $1 \mu\text{m}$ thick and most of the damage is introduced at the end of the range, which is at $12 \mu\text{m}$ for 12 MeV C. The energy loss in the ΔE part of the detector is about 1 MeV, with the majority being electronic energy loss and less than 0.1% nuclear energy loss, which causes the damage. On the other hand the nuclear stopping is two orders of magnitude larger at the end of range of the ions. This is reflected in the ΔE , which show only a minimal change with ion irradiation. Even after 10^5 ions into a $2 \times 2 \mu\text{m}^2$ spot the ΔE peak shifts by less than 3%. This shows that even for high energy ions the deterioration of the ΔE detector due to ion damage is less of concern.

Although the spectra in Fig. 2 represent the impact of 1.5×10^5 ions on the sample, the damage in this case is minimised by scanning the beam over an area of $70 \times 70 \mu\text{m}^2$. This reduces the real density and damage by three orders of magnitude. Hence the effect of ion beam damage is minimal, consistent with Fig. 4 which shows that up to a fluence of 0.5×10^{12} ions/ cm^2 the damage is small and the peak shift is less than 10%.

Fig. 5(a) shows ΔE – E coincidence spectra taken at the ΔE anode in the lower right corner of the device using a 3 MeV He beam. For comparison the coincidence spectrum taken at the common cathode in the lower left corner is shown in Fig. 5(b). This spectrum is similar to the coincidence spectrum taken in the centre of the device. However, the pure E detector spectrum from this part of the device is different from the spectrum in the centre of the device. Fig. 6 shows this energy spectrum. The reason why the difference does not appear in the coincidence spectrum is that events outside the active region do not create an event in the ΔE part of the detector. Therefore these events do not appear in the coincidence spectrum. Using the coincidence spectrum to select only events in region 1 of Fig. 5(b), the energy spectrum is identical to energy spectrum in the central region. This energy spectrum is also

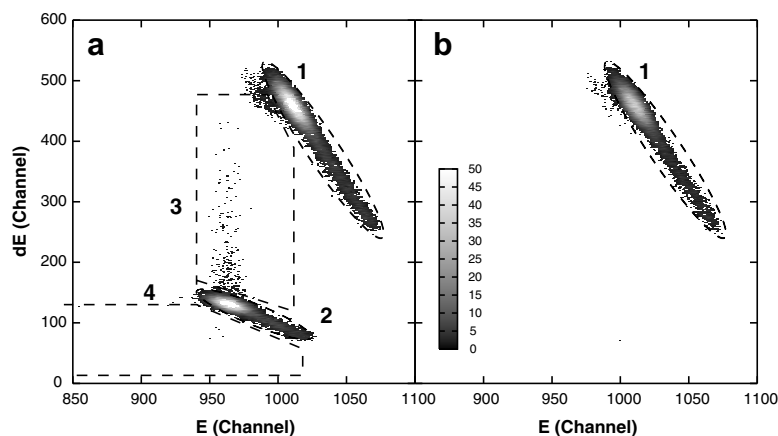


Fig. 5. ΔE – E coincidence spectra taken at the ΔE anode in the lower right corner of the device with 3 MeV He^{2+} (a) and at the common cathode in the lower left corner (b).

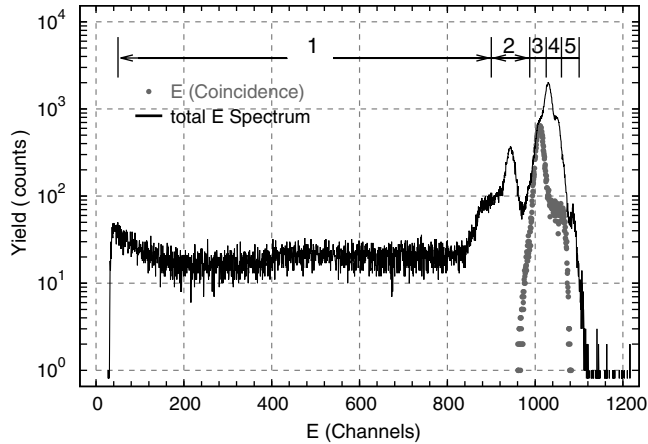


Fig. 6. Spectrum of the E detector from the coincidence spectrum of Fig. 5(b) and total E spectrum. The energy windows for the cuts shown in Fig. 7 are indicated in the figure.

shown in Fig. 6. This demonstrates how the ΔE – E device can be used to discriminate against events from outside the active region.

To determine, from which location on the device different parts of the energy spectrum originate, energy slices were mapped as a function of the beam position. Fig. 7 shows maps for different energy slices of the E signal, indicated in Fig. 6. The map on the left represents the lowest energy, while the map on the right is for the high energy part. The maps clearly show the different parts of the device visible in the electron micrograph. The map in the middle

represents the energy region in the spectrum selected from the coincidence spectrum. However, this map also shows areas outside the active region, which shows that selecting a region from the E spectrum, includes events from outside the active area. Higher energy events come from the common p^+ cathode contact pad for both detector parts and the ring around the device. In this part of the device, the deposited beam energy is higher, because the ΔE stage has been removed. The images also show the contact wire, which completely stops the ion beam.

The coincidence spectrum of Fig. 5(a) shows additional features, which are due to the additional structure in this part of the device. Similar to the spectrum in Fig. 5(b), the coincidence spectrum shows the main peak with a tail toward lower energies in ΔE and higher energies in E , indicated by the region 1. A similar peak can be seen at slightly lower E and a fifth of the ΔE signal (region 2). Mapping events in the regions indicated in Fig. 5(a) results in the maps of Fig. 8. The first map of Fig. 8 shows events from region 1 again showing the active region. The second map shows events from region 2, resulting from ions hitting the ΔE anode of the detector. The region between, the two peaks (region 3), is shown in the third map, which shows the border between the active region and the ΔE anode. Region 4 is shown in map 4, which is the outside border of the ΔE anode, resulting in low charge collection in both E and ΔE .

The coincidence spectrum shows that the signal from the E detector in the region of the ΔE anode is lower than the signal from the active region, which is due the additional

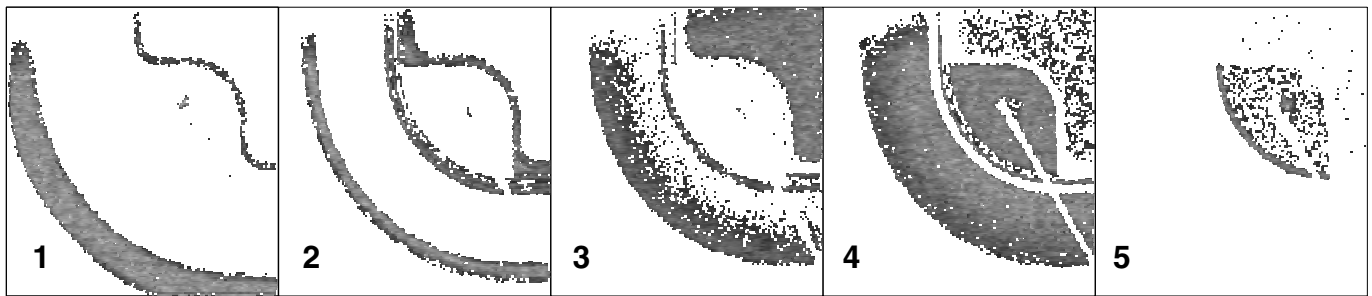


Fig. 7. Maps representing different energy slices of the total energy spectrum (see Fig. 6) taken at the common cathode in the lower left corner of device.

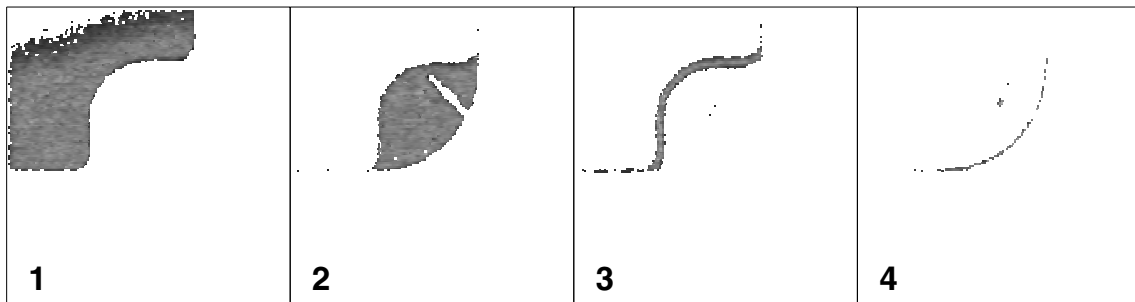


Fig. 8. Maps generated from the ΔE – E coincidence spectrum of Fig. 5(a), using the marked regions taken at the ΔE cathode in the lower right corner of the device.

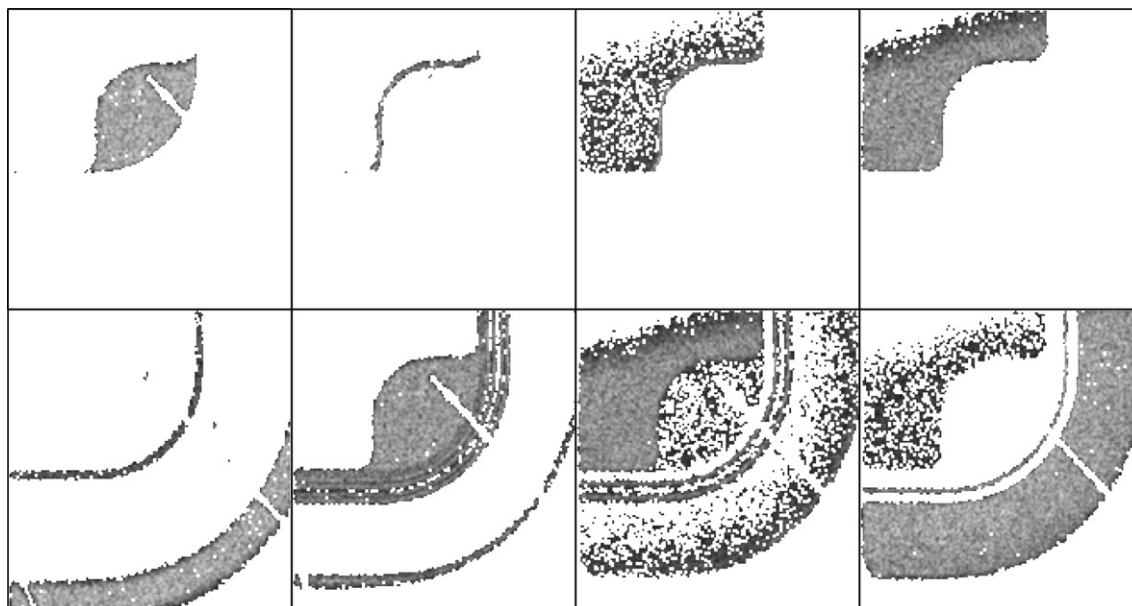


Fig. 9. Maps generated from cuts of the ΔE spectrum (top row) and the E spectrum taken at the ΔE anode in the lower right corner of the device.

energy loss of the beam in the metal contact at the anode. The additional energy loss is approximately 150–200 keV, which is equivalent to a 0.7–1.0 μm thick Al layer of the contact pad. This additional Al layer should reduce the channeling in this region, compared to active region of the device [10]. Surprisingly, the ratio between peak and tail from both regions are almost the same. However, channeling can only be ruled out as the cause of the tails, by measuring the response of the device at different tilt angles.

Comparing the ΔE signal from the two regions, the ΔE signal from the contact pad region is much lower. This may be explained by an edge effect with poor charge collection.

For comparison the maps generated from energy cuts of the ΔE and E spectra are shown in Fig. 9. The top row shows maps generated from the ΔE detector, while the bottom row is from the E detector. Not surprisingly the maps from the ΔE detector are identical to the maps generated from the coincidence spectrum. However, the maps from the E spectrum, show like the maps of Fig. 7 additional features of the device. In contrast to Fig. 7 in this case the contact pad appears at a lower energy. This is due to the additional energy loss in the contact layer on top.

4. Conclusions

We have used coincidence measurements to characterise a ΔE – E telescope using various ions such as H, He and C. The ΔE – E coincidence spectra show tails for all ion species (except H), with a peak to tail ratio that is independent of the ion species and the thickness of the overlayer. This behaviour is still under study.

Mapping shows that the response of the detector can be directly linked to various parts of the detector and the influence of the layered structure of the device.

Artefacts from the ΔE -pad region are clearly highlighted by the IBIC characterisation and the problem will be fixed in a future design. Nevertheless the device can still be used if the active region is selected using an aperture.

The measurements show that the ΔE stage is less sensitive to radiation damage than the E stage of the detector.

Acknowledgment

The authors would like to acknowledge the efforts of the Acceleration Operations Team at ANSTO and the technical staff of the Nuclear Engineering Dept. of Politecnico di Milano.

References

- [1] J.F. Dicello, H.I. Amols, M. Zaider, G. Tripart, *Radiat. Res.* 82 (1980) 441.
- [2] P.D. Bradley, A.B. Rosenfeld, M. Zaider, *Nucl. Instr. and Meth. B* 184 (2001) 135.
- [3] S. Agosteo, P.G. Fallica, A. Fazzi, A. Pola, G. Valvo, P. Zotto, *Appl. Radiat. Isotopes* 63 (2005) 529.
- [4] F. Sexton, K. Horn, B. Doyle, M. Shaneyfelt, T. Meisenheimer, *IEEE Trans. Nucl. Sci.* 42 (6) (1995) 1940.
- [5] H. Legge, *Nucl. Instr. and Meth. B* 130 (1997) 9.
- [6] R. Siegele, D.D. Cohen, N. Dytlewski, *Nucl. Instr. and Meth. B* 158 (1999) 31.
- [7] Iwan M. Cornelius, Anatoly B. Rosenfeld, Rainer Siegele, Anatoly B. Rosenfeld, David D. Cohen, *IEEE Trans. Nucl. Sci.* 50 (6) (2003) 2373.
- [8] Iwan M. Cornelius, Rainer Siegele, Ivo Orlic, Anatoly B. Rosenfeld, David D. Cohen, *Nucl. Instr. and Meth. B* 210 (2003) 191.
- [9] Iwan M. Cornelius, Rainer Siegele, Anatoly B. Rosenfeld, David D. Cohen, *IEEE Trans. Nucl. Sci.* 49 (2002) 2805.
- [10] E. Lugujo, J.W. Mayer, *Phys. Rev. B* 7 (5) (1973) 1782.